Chemical Engineering Journal 157 (2010) 598–604

Contents lists available at ScienceDirect

Chemical Engineering Journal

journal homepage: www.elsevier.com/locate/cej

Preparation of Glycy-L-Tyrosine intercalated layered double hydroxide film and its *in vitro* release behavior

Xianggui Kong, Shuxian Shi, Jingbin Han, Fengjie Zhu, Min Wei*, Xue Duan

State Key Laboratory of Chemical Resource Engineering, Beijing University of Chemical Technology, Beijing 100029, China

ARTICLE INFO

Article history:
Received 9 September 2009
Received in revised form 11 January 2010
Accepted 11 January 2010

Keywords:
GlyTyr
Layered double hydroxide
Intercalation
GlyTyr-LDH film
In vitro release

ABSTRACT

This paper describes the preparation of films of peptide (Glycy-L-Tyrosine, denoted as GlyTyr) intercalated layered double hydroxide (LDH) and its release performances. GlyTyr has been intercalated into a magnesium–aluminum LDH, and the resulting film was fabricated by solvent evaporation method in order to exploit new formulation in drug carrier especially used in skin medicament. Based on the results of XRD, FT-IR, FT-IR-ATR, UV–vis, ^{13}C NMR, ICP and elemental analysis, it was found that GlyTyr has been successfully intercalated into LDH gallery. TG/DTA, *in situ* FT-IR, *in situ* XRD and polarimetry indicate that the chemical stability of GlyTyr was enhanced significantly in the confined region of LDH galleries compared with its pristine form. SEM reveals that the film thickness is about 12.6 μm with *c*-orientation of LDH platelets (*ab* plane parallel to the substrate). *In vitro* release tests of the GlyTyr-LDH film in pH 7.4 phosphate buffered saline (PBS) showed that no burst release phenomenon occurred at the beginning stage and a high release ratio of GlyTyr (91%) was obtained, exhibiting controlled release behavior. Furthermore, the parabolic diffusion model was used to simulate the release kinetics of GlyTyr from the LDH carrier, indicating that the external surface diffusion or the intraparticle diffusion *via* ion-exchange is the rate-determining step in the release process. Therefore, this work demonstrates that Mg/Al-LDH is an effective inorganic matrix for the peptide storage and controlled delivery at the required time.

1. Introduction

Many drugs are poor water-solubility, leading to difficulties in efficient dose delivery and unwanted side effects. Additionally, there are many cases where conventional drug administration methods do not provide satisfactory pharmacokinetic profiles because the drug concentration rapidly falls below desired levels. Therefore, drug research is currently moving towards the controlled drug release, which offers numerous benefits in medicament, by retaining drug bioactivity, reducing side effects, prolonging duration time, balancing drug concentrations within a desired range and facilitating to the patient [1–3]. Furthermore, preparation of surface coatings or thin films from nanostructure materials with controlled release performances plays an important role in drug release system [4]. Inorganic materials possess many advantages as drug carriers, for example, they have hydrophilic surfaces that increase their circulation time in blood; they exhibit good properties of stability, biocompatibility and ease of surface modification. Moreover, they can be prepared as solids, colloids and thin films to meet different needs [5]. Taking into account these aspects, inorganic materials including layered materials and composites [6], open framework materials [7] and metal oxides in the form of nanoparticles [8] have drawn extensive attention and obtained huge success over the past decades in drug delivery and controlled release systems.

Layered double hydroxides (LDHs), one family of promising inorganic solid matrixes [9–13], can be described by the general formula $[M^{2+}_{1-x}M^{3+}_{x}(OH)_2]^{x+}(A^{n-})_{x/n}\cdot mH_2O$, where M^{2+} and M^{3+} are divalent and trivalent metal ions, respectively, and A^{n-} is an exchangeable anion compensating for the positive charge of the hydroxide layers [14]. Recently, some biocompatible LDHs have attracted considerable attention as drug delivery materials due to the following advantages: easy preparation, low cost, good biocompatibility, low cytotoxicity, full protection for the intercalated drugs and good suitability in cellular and animal systems [15,16]. In order to demonstrate the feasibility of LDH-based drug delivery systems, a series of pharmaceutically active compounds, such as ibuprofen, diclofenac, gemfibrozil, naproxen, 2-propylpentanoic acid, 4-biphenylacetic acid and tolfenamic acid, etc., have been intercalated into LDHs [17–19]. Furthermore, the negatively charged

* Corresponding author at: Beijing University of Chemical Technology, Science College, Box 98, Beisanhuan East Road, Chaoyang Dis., Beijing 100029, China. Tel.: +86 10 64412131; fax: +86 10 64425385.
E-mail addresses: weimin@mail.buct.edu.cn, weimin-hewei@163.com (M. Wei).

1385-8947/$ – see front matter © 2010 Elsevier B.V. All rights reserved.
doi:10.1016/j.cej.2010.01.016

drugs in the gallery space of LDHs would gain extra stabilization energy owing to the host–guest interactions, and thus their biological activity and stability can be enhanced significantly. It has been reported that the drug–LDH composites showed high chemical stability and even can be maintained as long as 4 years [20].

GlyTyr, a kind of dipeptide, is an important source of tyrosine in animal and human body, which plays a crucial role in treating renal failure, easing the adverse effects of stress, hypertension and dementia [21]. Additionally, it can also serve as precursor for some superior drugs. However, both the chemical and stereochemical stabilities of GlyTyr are unstable, and its oxidation, decomposition as well as racemization occur easily under mild conditions [22]. All these disadvantages mentioned above restrict the use of GlyTyr. As a result, searching drug delivery and controlled release system is an effective solution for overcoming such problems.

In our previous work, chiral drugs L-dopa and L-tryosine [23] were successfully intercalated into the gallery of LDH and the results showed that their thermal and chiral stabilities were improved remarkably after intercalation. In this work, we further studied the intercalation of GlyTyr into MgAl-LDH and investigated the influences of host–guest interactions on its properties by *in situ* XRD, *in situ* FT-IR and TG-DTA. Moreover, films of GlyTyr-LDH have been fabricated by a solvent evaporation method in this work, for the purpose of exploring its new type of controlled release formulation for drug. Films of drug system would be ideal for delivery of drugs in the oral cavity or in skin, due to its flexibility and comfort relative to adhesive tablets. It can also circumvent the relatively short residence time of oral gels on the mucosa, which is easily washed away and removed by saliva [24]. Many studies on polymer films as drug carrier have been reported in recent years [25,26], but the side effects of organic matrixes cannot be neglected. In this work, inorganic film of GlyTyr-LDH with good biocompatibility was prepared, and its application as a novel release formulation for drug was investigated. The *in vitro* release behavior of GlyTyr from the film formulation was studied, and the results show that this drug–LDH film exhibits a high release ratio (91%) in pH 7.4 PBS solution. Therefore, it is expected that the LDH-based inorganic film in this work can serve as a feasible peptide carrier for the potential applications in cosmetic such as skin protection, transdermal therapy and tissue regeneration.

2. Experimental

2.1. Materials

GlyTyr (purity ≥99.7%) was purchased from Sigma–Aldrich and used as received. Other inorganic chemicals including $Mg(NO_3)_2{\cdot}6H_2O$, $Al(NO_3)_3{\cdot}9H_2O$, Na_2CO_3 and NaOH, were purchased from the Beijing Chemical Co. Limited and used without further purification. The deionized and de-CO_2 water was used in all the experimental processes.

2.2. Preparation of GlyTyr-LDH powder

NO_3–MgAl/LDH precursor was synthesized by the hydrothermal method reported previously [27]. GlyTyr-LDH was prepared using a coprecipitation method. A mixed solution (50 ml) of 0.2 M $Mg(NO_3)_2{\cdot}6H_2O$ and 0.1 M $Al(NO_3)_3{\cdot}9H_2O$ was added dropwise to a solution (50 ml) of 1.0 M NaOH and 0.3 M GlyTyr with vigorous agitation under a nitrogen atmosphere. The mixture was aged at 65 °C for 24 h after the solution pH was adjusted to 9.0 by 1.0 M NaOH. The resultant suspension was separated and washed thoroughly using deionized water, and dried at 70 °C for 24 h.

2.3. Preparation of GlyTyr-LDH film

Thin films of GlyTyr-LDH were fabricated by the solvent evaporation method. The GlyTyr-LDH powder (0.05 g) was suspended in water (20 mL) and treated in an ultrasonic bath (99 W, 28 kHz) under N_2 atmosphere for 5 min. After filtration using a membrane filter (0.2 μm, Millipore, in order to obtain uniform LDH particles), 5 mL of GlyTyr-LDH suspension was dropped onto quartz substrates (1 cm × 3 cm, 0.013 g of GlyTyr-LDH) and dried in vacuum at 70 °C for 24 h. All the quartz substrates were pretreated in an aqueous H_2O–NH_4OH (3:7, v/v) solution for 30 min, followed by a thorough rinsing with deionized water.

2.4. In vitro GlyTyr release test from GlyTyr-LDH film

A multipoint working curve was made. A series of solutions in simulated intestinal fluids (phosphate buffers with pH 7.4) with the concentration of GlyTyr in the range 0–100 ppm were prepared. The UV absorbance of the solution at 275.0 nm was plotted *vs*. the concentration of GlyTyr, and the multipoint linear working curve was obtained: conc. = $0.2461A - 0.0362$, where $R = 0.99989$.

Drug release tests were carried out at constant temperature (37 °C) by immersing the film on quartz substrate in a quartz cell with 5 ml of phosphate buffered saline (PBS, pH 7.4). The released GlyTyr was measured at predetermined time by UV–vis absorbance at 275.0 nm. In order to determine the drug content corresponding to total release, Na_2CO_3 (0.53 g) was dissolved in a suspension with the above composition and the mixture was shaken for 2 h, and the concentration of GlyTyr was also measured by the method described above. After the release test, the GlyTyr-LDH film was washed and dried at 70 °C for 24 h in vacuum, followed by the measurement of XRD. This residue was named as GlyTyr-LDH-R film.

2.5. Characterizations

Powder X-ray diffraction (XRD) patterns were recorded on a Rigaku XRD-6000 diffractometer using Cu Kα radiation (λ = 0.154 nm) at 40 kV, 30 mA, a scanning rate of 5° min^{-1}, and a 2θ angle ranging from 3° to 70°. The Fourier transform infrared (FT-IR) spectra were recorded using a Vector 22 (Bruker) spectrophotometer in the range 4000–400 cm^{-1} with 2 cm^{-1} resolution. The standard KBr disk (1 mg of sample in 100 mg of KBr) was used. The UV–vis spectra were recorded on a Shimadzu UV-2501PC spectrometer in the wavelength range 200–700 nm, and the quantitative analysis was performed at 275.0 nm. Microanalysis of metals was performed by inductively coupled plasma (ICP) emission spectroscopy on a Shimadzu ICPS-7500 instrument using solution prepared by dissolving the samples in dilute HNO_3. Carbon, Hydrogen and nitrogen analyses were carried out using an Elementarvario elemental analysis instrument. Solid-state ^{13}C nuclear magnetic resonance (NMR) spectra were run on a Bruker AV300 spectrometer operating at a frequency of 75.467 MHz for ^{13}C with a 5 s pulse delay. The *in situ* FT-IR spectra were recorded using a Niclet 560 FT-IR spectrophotometer in the temperature range 25–285 °C with a heating rate of 5 °C/min. The *in situ* XRD measurements were performed on a PANalytical X' Pert PRO MPD diffractometer in the temperature range 25–505 °C under vacuum using Cu kα radiation (λ = 0.154 nm) at 45 kV, 35 mA. Scanning rate was 10 °C/min, and the rate of temperature increase was 50 °C/min with a holding time of 3 min before each measurement. TG-DTA (30–700 °C) was measured on a HCT-2 thermal analysis system under normal atmosphere with a heating rate of 10 °C/min. Optical rotation measurements were carried out on a WZZ-1S automatic polarimeter at 589.3 nm (Na D-line). The SEM micrograph was recorded on a Hitachi S-3500N scanning electron microscope.

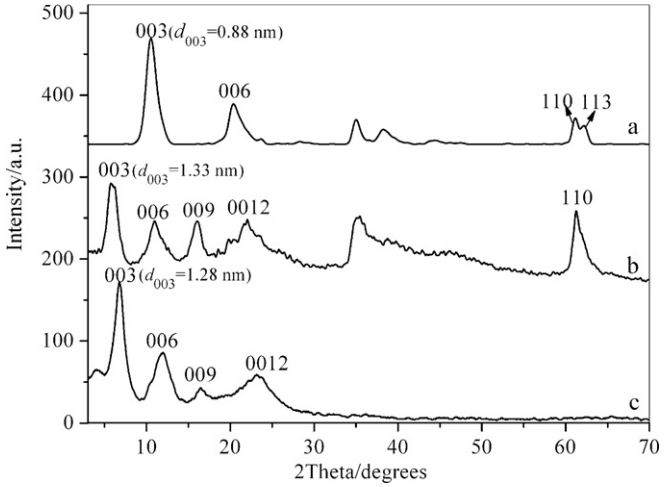

Fig. 1. XRD patterns of (a) NO_3–MgAl/LDH, (b) GlyTyr-LDH powder sample and (c) GlyTyr-LDH film.

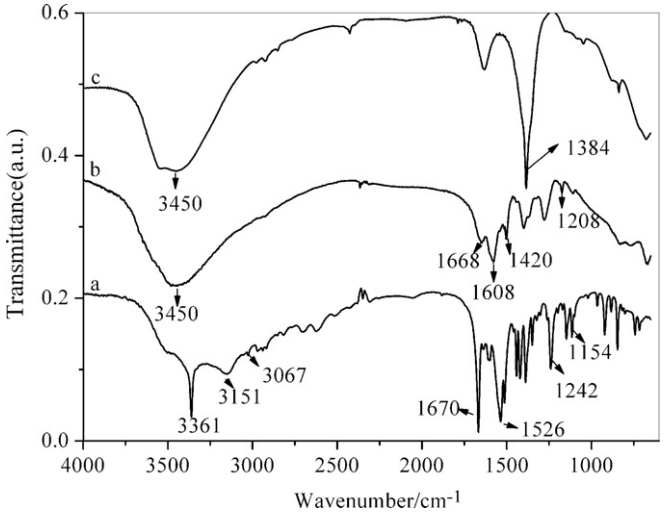

Fig. 2. FT-IR spectra for (a) pristine GlyTyr, (b) GlyTyr-LDH powder and (c) NO_3–MgAl/LDH.

3. Results and discussion

3.1. Characterization of GlyTyr-LDH composite

The powder XRD patterns of the NO_3–MgAl/LDH precursor and the product GlyTyr-LDH are shown in Fig. 1. In each case, the reflections can be indexed to a hexagonal lattice with *R*-3*m* rhombohedral symmetry, which often used for the description of LDH structures [28]. The basal diffraction (0 0 3) of the GlyTyr-LDH (Fig. 1b, $2\theta = 6.64^\circ$, $d_{003} = 1.33$ nm) shifted to a lower angle compared with that of NO_3–MgAl/LDH (Fig. 1a, $2\theta = 10.38^\circ$, $d_{003} = 0.88$ nm), indicative of intercalation of GlyTyr into LDH gallery. Moreover, the (1 1 0) reflection ($2\theta = 61^\circ$) showed no obvious shift, indicating that no significant change occurred in the LDH host layers along with intercalation of GlyTyr. In the case of the GlyTyr-LDH film (Fig. 1c), a series of reflections (h, $k \neq 0$) at high angle disappeared as expected, which is an evidence for an extremely well *c*-oriented assembly of LDH platelets in the film [29]. However, it can be seen that the (0 0 3) reflection of the film sample moved to higher 2θ value compared with its powder sample. This might be related to the different content of interlayer water between the two samples, although the drying temperatures are the same during the synthesis process. The content of interlayer water imposes influence on the interlayer distance, which will be confirmed by the *in situ* high-temperature XRD in the next section. Moreover, the edge view of SEM image (Fig. S1A) shows that the film thickness is about 12.6 μm with *c*-orientation of LDH platelets (*ab* plane parallel to the substrate). This is consistent with the XRD result in Fig. 1c. As shown in Fig. S1B, no delamination or peeling occurred upon cross-cutting the surface, indicating high stability of the film.

The FT-IR spectra of the solid products are shown in Fig. 2. For the sake of clarity only the main absorption bands were listed. In the spectrum of GlyTyr (Fig. 2a), the bands at 3361, 3151 and 3067 cm^{-1} can be attributed to ν(N–H), ν(O–H) and ν(Ar–H) vibrations, respectively. The bands centered at 1670 and 1242 cm^{-1} belong to C=C, C–N stretching vibrations and those at 1526 and 1154 cm^{-1} due to δ(N–H) and δ(O–H) deformation modes, respectively. The spectrum of NO_3–MgAl/LDH precursor (Fig. 2c) shows a broad absorption band at 3450 cm^{-1} due to the stretching vibration of the hydroxyl group in the LDH layers and interlayer water molecules. The band at 1384 cm^{-1} belongs to the stretching vibration of NO_3^-. In the case of GlyTyr-LDH (Fig. 2b), the broad absorption peak at about 3450 cm^{-1} is assigned to O–H group stretching and deformation vibration of the hydroxide basal and interlayer water molecule. Moreover, some characteristic bands of GlyTyr were observed at 1668, 1608, 1420 and 1208 cm^{-1}. Meanwhile, the band at 1384 cm^{-1} assigned to the stretching vibration of NO_3^- disappeared, indicating that GlyTyr has been successfully intercalated into LDH gallery. Furthermore, Fig. 3 displays the FT-IR-ATR spectra of pristine GlyTyr, GlyTyr-LDH powder and GlyTyr-LDH film sample, respectively. In Fig. 3a, the strong bands at 2850 and 2915 cm^{-1} belong to $\nu(CH_2)$; bands at 1653 and 1543 cm^{-1} are attributed to absorption of amide group. All these typical bands were observed in the GlyTyr-LDH powder and film samples (Fig. 3b and c). Both the FT-IR and FT-IR-ATR results confirm that the chemical structure of GlyTyr remains unchanged in the GlyTyr-LDH powder and film samples.

Solid-state ^{13}C NMR was used to further confirm the intercalation of GlyTyr into LDH gallery. The spectrum of GlyTyr (Fig. 4a) displays the resonances at 33 ppm C(1), 178 ppm C(2), 43 ppm C(3), 166 ppm C(4), 55 ppm C(5), 155 ppm C(6), 132 ppm C(7, 8), 130 ppm C(9, 10) and 115 ppm C(11). Compared with pristine GlyTyr, all the resonances in the spectrum of GlyTyr-LDH (Fig. 4b) shifted downfield by ca. 4 ppm, especially C(4) (by ca. 11 ppm), which is related to the host–guest interactions (including electrostatic attraction and

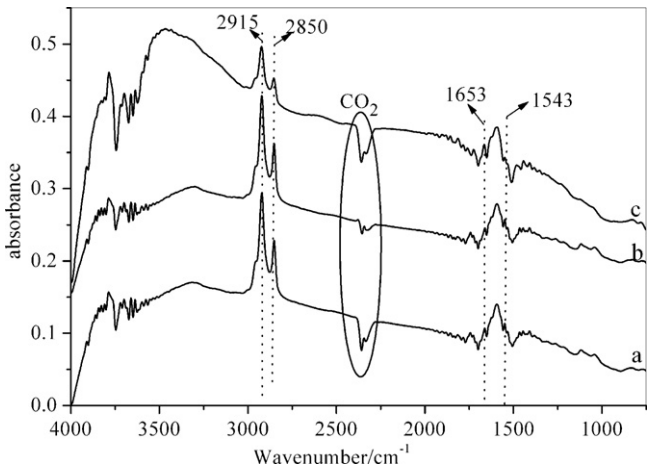

Fig. 3. FT-IR-ATR spectra for (a) pristine GlyTyr, (b) GlyTyr-LDH powder and (c) GlyTyr-LDH film.

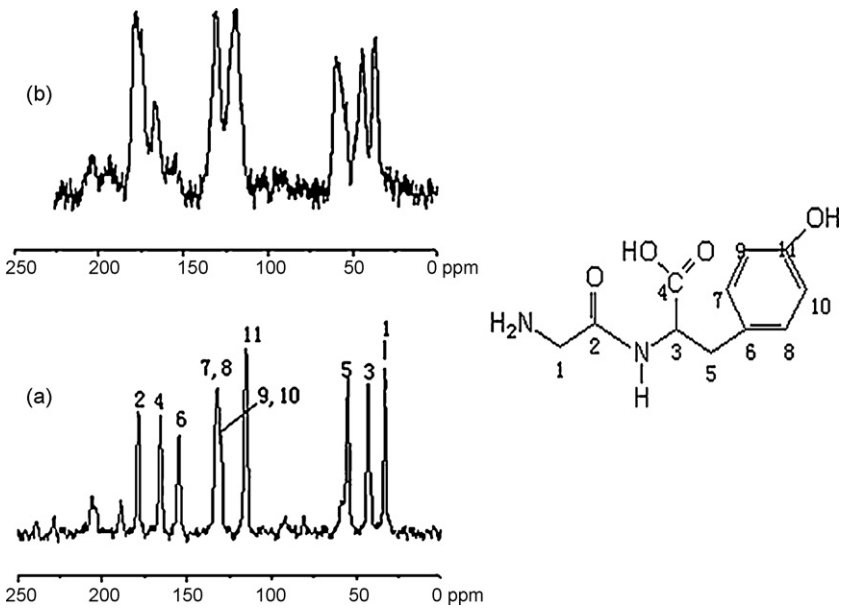

Fig. 4. Solid-state ^{13}C NMR spectra of (a) pristine GlyTyr and (b) GlyTyr-LDH powder.

hydrogen bonding). Based on the results above, it can be concluded that GlyTyr has been intercalated into the gallery of LDH.

In order to demonstrate whether the GlyTyr still keeps its stereochemical structure in the gallery space of LDH, the optical rotation of GlyTyr before and after intercalation into Mg/Al-LDH was measured. It was found that the value of specific optical rotation for the intercalated GlyTyr ($\alpha^{20}_{589.3} = 47.6^{\circ}$, 1 M HCl) does not decrease obviously compared with that of the pristine GlyTyr ($\alpha^{20}_{589.3} = 48.7^{\circ}$, 1 M HCl), indicating that no racemization of GlyTyr occurs during the intercalation process. According to the elemental analysis data: Mg 16.8%, Al 8.58%, C 18.0%, H 4.92%, N 3.56%, the Mg^{2+}/Al^{3+} molar ratio determined experimentally for the composite is 2.2, which is approximately equal to the nominal ratio (2.0). The C/N ratio (5.9) is larger than that of pure GlyTyr (5.5, based on the molecular formula $C_{11}H_{14}N_2O_4$), indicating little amount of CO_3^{2-} coexisting in the gallery. Based on the elemental data, the chemical formula of GlyTyr-LDH can be expressed by $Mg_{0.68}Al_{0.32}(OH)_2(C_{11}H_{13}N_2O_4)_{0.18}(CO_3)_{0.07}\cdot 1.25H_2O$. The content of intercalated GlyTyr anions accounts for 56.2% (molar percentage) in the total guest anions, relative to the chemical composition of CO_3-LDH ($Mg_{0.68}Al_{0.32}(OH)_2(CO_3)_{0.16}\cdot 0.10H_2O$).

3.2. The structural model

On the basis of the basal spacing d_{003} of 1.33 nm for the GlyTyr-LDH observed by XRD, and subtracting the thickness of brucite layer (0.48 nm), the gallery height is calculated to be 0.85 nm, smaller than the length of GlyTyr (1.12 nm × 0.51 nm × 0.45 nm, calculated with quantum chemistry at B31YP/6-31G (d,p) level). By virtue of the presence of one carboxyl group, two amino groups and one hydroxyl group in its structure, GlyTyr shows a three-step ionization in water solution ($pKa_1 = 2.93$, $pKa_2 = 8.45$, $pKa_3 = 10.49$). According to the synthesis condition of pH 9.0 in the coprecipitation process, the distribution coefficient of the monovalent anion was calculated to be 77.3%, indicating its overwhelming majority in the interlayer gallery of LDH. Therefore, it is proposed that the GlyTyr anions are accommodated in the interlayer region as a monolayer of species with the carboxyl of individual anions alternately attaching to the upper and lower hydroxide layers. The host–guest interactions consist of electrostatic attraction between the positively charged host layers and negatively charged guests, as well as the hydrogen bonding formed among host layers, guest anions and interlayer water molecules. The schematic representation of the probable arrangement for GlyTyr-LDH is shown in Fig. 5.

3.3. Investigation of thermal stability of GlyTyr-LDH

The *in situ* XRD patterns of the intercalation product in the temperature range 25–505 °C are presented in Fig. 6. It can be observed that the (0 0 3) reflection of GlyTyr-LDH moved to higher angle

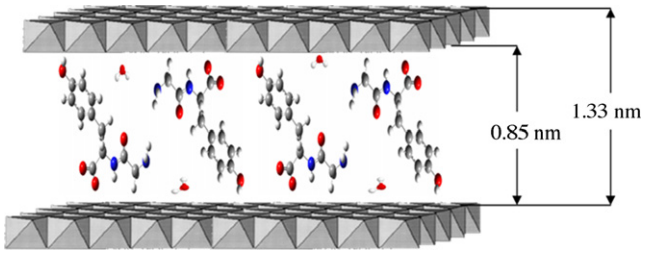

Fig. 5. A possible schematic representation for the GlyTyr-LDH.

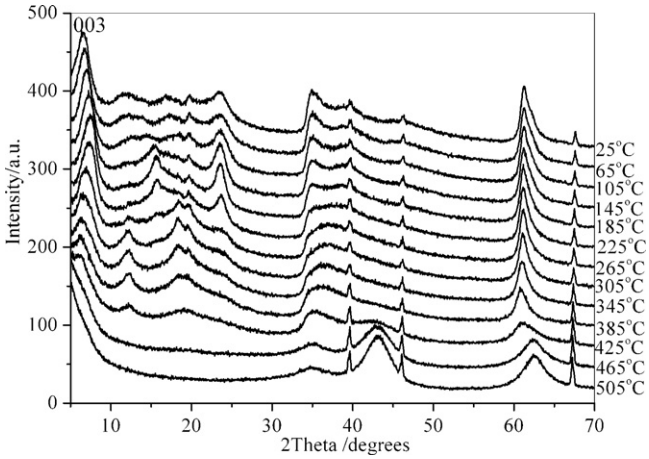

Fig. 6. *In situ* XRD patterns for the thermal decomposition of GlyTyr-LDH in the temperature range 25–505 °C.

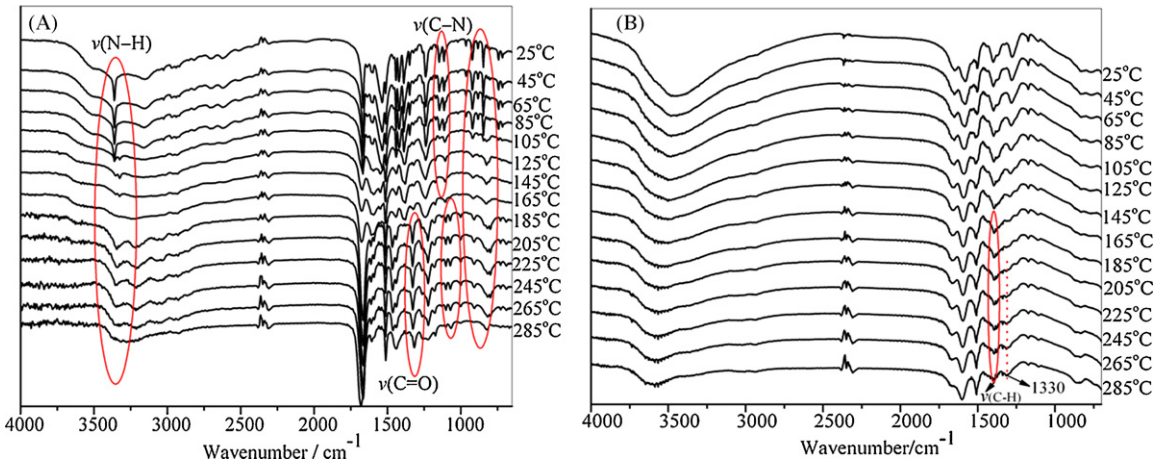

Fig. 7. *In situ* FT-IR spectra for the thermal decomposition of (A) pristine GlyTyr and (B) GlyTyr-LDH.

2θ upon increasing temperature. Correspondingly, the d_{003} basal spacing decreased from 1.33 nm (25 °C) to 1.09 nm (185 °C). The observed contraction (0.24 nm) can be attributed to the loss of hydrogen bonding resulting from the deintercalation of interlayer water molecules, for it is approximately close to the dimension of the hydrogen bonding space (0.22 nm) [23b]. Additionally, the (0 0 3) reflection of GlyTyr-LDH moved to lower angle from 185 to 305 °C, possibly due to the occurrence of condensation reaction of GlyTyr anions. This will be further confirmed by the *in situ* FT-IR spectra (Fig. 7B). Moreover, the intensity of (003) reflection significantly declined from 225 to 305 °C, due to the decomposition of the guest and partial dehydroxylation of the host layer. As the temperature rose to 465 °C, the complete decomposition of interlayer guest and collapse of the layered structure occurred, as shown by the disappearance of characteristic reflections of LDH and the observation of MgO reflections at 46.1° and 62.8°.

Besides the *in situ* XRD patterns, *in situ* FT-IR was used to record the infrared spectra during the decomposition process. For pristine GlyTyr (Fig. 7A), the first change occurred between 25 and 105 °C. The bands of ν(C=O) at 1670 cm^{-1}, ν(C–N) at 1242 cm^{-1} and ν(N–H) at 3361 cm^{-1} disappeared at 105 °C, indicating that GlyTyr began to decompose at this temperature. Furthermore, two new absorption bands at 1330 and 1230 cm^{-1} corresponding to amine appeared at the temperature of 185 °C, indicative of condensation reaction occurred between GlyTyr anions. In contrast, in the case of GlyTyr-LDH (Fig. 7B), no significant change in the main absorption bands of GlyTyr was observed between room temperature and 145 °C, indicating that the intercalated guest is stable in this temperature range. However, the band intensity (ν_{C-H} of the methyl at about 1375 cm^{-1}) decreased remarkably as the temperature increased from 165 to 285 °C, implying that the decomposition of intercalated GlyTyr begins at 165 °C. In addition, a new band at about 1330 cm^{-1} belongs to amine appeared at the temperature of 205 °C, indicating the condensation reaction of GlyTyr anions. The results reveal that the thermal stability of GlyTyr was improved when intercalated into LDH gallery.

The thermal decomposition of GlyTyr and GlyTyr-LDH was also studied by TG-DTA (Supporting Information Fig. S2). The GlyTyr used as a reference sample (Fig. S2A) exhibits a sharp exothermic peak at 172 °C in its DTA curve indicates that condensation reaction occurred at this temperature, in accordance with the result from *in situ* FT-IR spectra (Fig. 7A). The sharp weight loss (300–550 °C) can be attributed to the combustion of GlyTyr, with a very broad exothermic peak observed at 520 °C in the DTA curve. In the case of GlyTyr-LDH (Fig. S2B), its thermal decomposition is characterized by three steps: the first from room temperature to 200 °C results from the removal of the external surface adsorbed and interlayer water molecules (ca. 5 wt%); the second one (200–350 °C) involving a gradual weight loss, is due to the decomposition of GlyTyr and dehydroxylation of the brucite-like layers; the third one shows a sharp weight loss (350–450 °C) with the corresponding exothermic peak at 420 °C in the DTA curve. Based on the results of *in situ* XRD, *in situ* FT-IR and TG-DTA, it can be concluded that the thermal stability of intercalated GlyTyr was enhanced significantly compared with its pristine form.

3.4. In vitro release behavior of the GlyTyr-LDH film

In drug transport vehicles fields, much attention was paid to LDH nanoparticles as drug carriers [17,18,30], but LDH-based film used as drug carrier has not been reported to the best of our knowledge. In this section, the inorganic film of GlyTyr-LDH used as a novel release formulation for drug was investigated. The GlyTyr release profile from GlyTyr-LDH film in PBS solution (pH 7.4) is shown in Fig. 8, in which a release behavior with an early fast release of GlyTyr (30% in the first 25 min) followed by a relatively slow release (91% in 290 min) was observed. The early fast release is possibly attributed to the release of GlyTyr anions from external part of the lamellar structure. Then the slow release is due to the exchange of drug in the internal part of the lamellae with anions in PBS. The extended time period for GlyTyr to release from LDH matrix is largely due

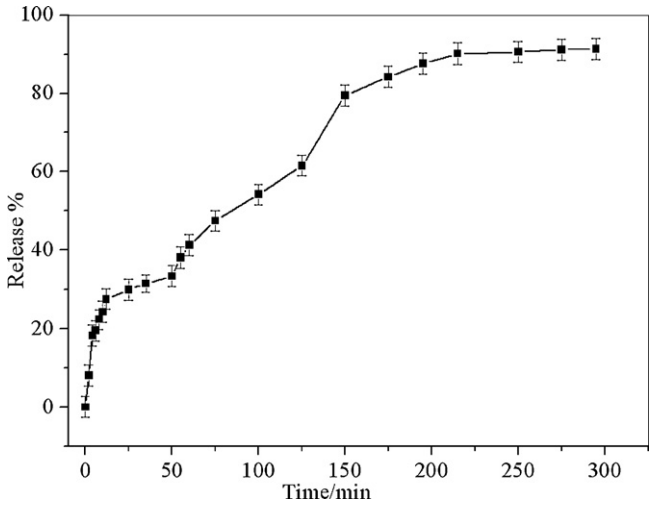

Fig. 8. Release profile of GlyTyr from the GlyTyr-LDH film in PBS solution (pH 7.4).

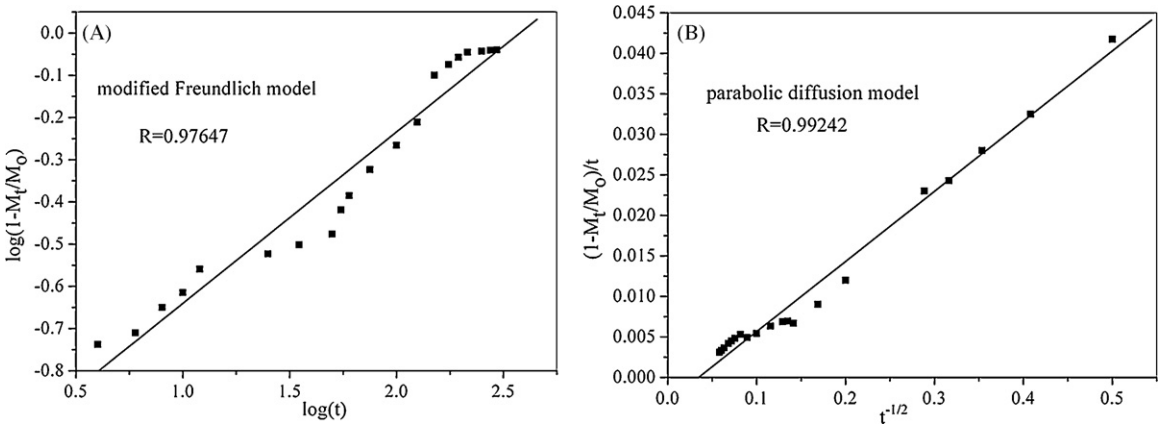

Fig. 9. Plots of the two kinetic models of (A) modified Freundlich model and (B) parabolic diffusion model for the release of GlyTyr from the LDH composite, respectively.

to the strong host–guest interactions. The mechanism of the drug release is very complex and not completely understood, which is generally classified as either purely diffusion or erosion controlled [31,32]. In order to further study the release behavior of GlyTyr from the LDH film, modified Freundlich model (Eq. (1)) [33] and parabolic diffusion model (Eq. (2)) [34] were chosen to investigate the release kinetics of this system:

$$\frac{M_0 - M_t}{M_0} = kt^a \quad (1)$$

$$\frac{(1 - M_t/M_0)}{t} = kt^{-0.5} + b \quad (2)$$

where M_0 and M_t are the drug content remained in the LDH film at release time 0 and t, respectively; k is the corresponding release rate constant, and a and b are constants whose chemical significance is not clearly resolved.

On the basis of the two kinetic models, the fitting results of drug release profiles are given in Fig. 9. It can be seen that the parabolic diffusion model can be better used to describe the drug release behavior (R = 0.99242) than the modified Freundlich model (R = 0.97647). Generally, the parabolic diffusion model elucidates that the release process is controlled by intraparticle diffusion or surface diffusion. Therefore, the simulation results indicate that the external surface diffusion or the intraparticle diffusion *via* ion-exchange is the rate-determining step in the release process.

To further confirm the release mechanism, the GlyTyr-LDH film after release was characterized by XRD, which still keeps its layered structure (Fig. 10b). Compared with the GlyTyr-LDH film (Fig. 10a, 2θ = 6.64°), the (003) reflection of GlyTyr-LDH-R film shifted to a larger angle (Fig. 10b, 2θ = 10.3°). The d_{003} value (0.89 nm) of the GlyTyr-LDH-R film accords with the basal spacing of phosphate anions intercalated LDH (d_{003} = 0.88 nm) [35]. As a result, the mechanism of GlyTyr-LDHs film release can be attributed to an ion-exchange process between GlyTyr anions and phosphate anions in the buffer. The morphology of the film was studied using SEM. The GlyTyr-LDH film exhibits a surprisingly smooth and continuous surface in the top view (Fig. S3A). In contrast, numerous small rifts in the GlyTyr-LDH-R film were observed (Fig. S3B), possibly owing to the contraction of interlayer distance of LDH during the ion-exchange process confirmed by XRD (Fig. 10b). The SEM image (Fig. S3B) shows that the GlyTyr-LDH film exhibits good corrosion resistance and strong adhesion to substrates during the release process.

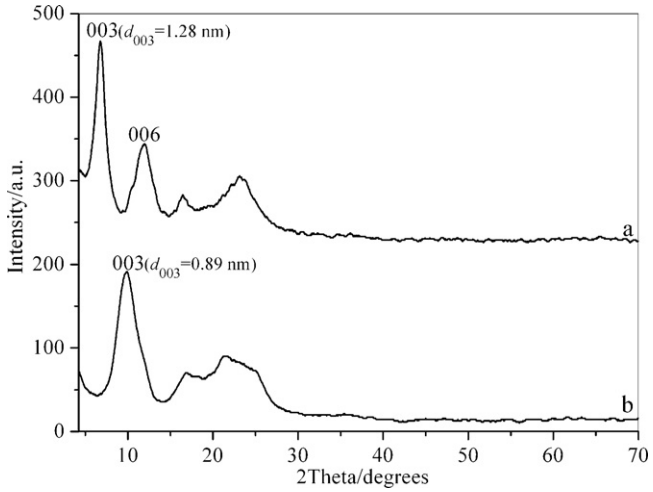

Fig. 10. The XRD patterns for (a) GlyTyr-LDH film and (b) GlyTyr-LDH-R film.

4. Conclusions

GlyTyr has been successfully intercalated into the LDH gallery by coprecipitation method, and the GlyTyr-LDH film with *c*-orientation was fabricated by solvent evaporation method. The results of *in situ* XRD, *in situ* FT-IR and TG-DTA exhibited that the thermal stability of GlyTyr was enhanced markedly when intercalated into LDH. No racemization of GlyTyr was observed after its incorporation into LDH through specific optical rotation measurement. Furthermore, the inorganic film as drug carrier was examined by *in vitro* release test, and the result showed that the GlyTyr-LDH film in PBS solution (pH 7.4) exhibits a release behavior, with an early fast release of GlyTyr followed by a relatively slow one. The release kinetics of GlyTyr from the LDH carrier was described by the parabolic diffusion model satisfactorily, indicating that the release process was controlled by the external surface diffusion or intraparticle diffusion. The host–guest interactions play an important role in the guest stability and drug release performances. It is anticipated that this inorganic film can serve as a promising material for drug delivery in therapeutic efficacy especially in surface coatings with controllable release properties.

Acknowledgments

This project was supported by the National Natural Science Foundation of China, the 111 Project (Grant No. B07004), the 973 Program (Grant No. 2009CB939802) and the Chinese Universities Scientific Fund (Grant No.: ZZ0908).

Appendix A. Supplementary data

Supplementary data associated with this article can be found, in the online version, at doi:10.1016/j.cej.2010.01.016.

References

[1] R. Langer, New methods of drug delivery, Science 249 (1990) 1527–1533.
[2] M. Manzano, V. Aina, C.O. Areán, F. Balas, V. Cauda, M. Colilla, M.R. Delgado, M. Vallet-Regí, Studies on MCM-41 mesoporous silica for drug delivery: effect of particle morphology and amine functionalization, Chem. Eng. J. 137 (2008) 30–37.
[3] X.T. Shuai, H. Ai, N. Nasongkl, S. Kim, J.M. Gao, Micellar carriers based on block copolymers of poly(ε-caprolactone) and poly(ethylene glycol) for doxorubicin delivery, J. Control. Release 98 (2004) 415–426.
[4] Q.M. Ji, M. Miyahara, J.P. Hill, S. Acharya, A. Vinu, S.B. Yoon, J.S. Yu, K. Sakamoto, K. Ariga, Stimuli-free auto-modulated material release from mesoporous nanocompartment films, J. Am. Chem. Soc. 130 (2008) 2376–2377.
[5] O.S. Tolulope, A.L. Vermeulen, Ultrasound-mediated release of $[Ru(bpy)_3]^{2+}$ from a layered titanate film—a model for controlled drug release from layered metal oxide films, J. Mater. Chem. 16 (2006) 2781–2784.
[6] A.I. Khan, D. O'Hare, Intercalation chemistry of layered double hydroxides: recent developments and applications, J. Mater. Chem. 12 (2002) 3191–3198.
[7] M. Valeet-Regi, A. Ramila, R.P. Del Real, J. Perez-Pariente, A new property of MCM-41: drug delivery system, Chem. Mater. 13 (2001) 308–311.
[8] (a) Y. Zhou, S.X. Wang, B.J. Ding, Z.M. Yang, Modification of magnetite nanoparticles via surface-initiated atom transfer radical polymerization (ATRP), Chem. Eng. J. 138 (2008) 578–585;
(b) Y.-Z. You, C.-Y. Hong, C.-Y. Pan, P.-H. Wang, Synthesis of a dendritic core–shell nanostructure with a temperature-sensitive shell, Adv. Mater. 16 (2004) 1953–1957.
[9] M. Verónica, B. Graciela, A. Norma, L. Miguel, Ethanol steam reforming using Ni(II)–Al(III) layered double hydroxide as catalyst precursor: kinetic study, Chem. Eng. J. 138 (2008) 602–607.
[10] J.M. Morris, S. Jin, K. Cui, Removal of endocrine active compounds using layered double hydroxide material, Chem. Eng. J. 145 (2008) 160–163.
[11] F. Leroux, J.P. Besse, Polymer interleaved layered double hydroxide: a new emerging class of nanocomposites, Chem. Mater. 13 (2001) 3507–3515.
[12] A.M. Fogg, J.S. Dunn, S.G. Shyu, D.R. Cary, D. O'Hare, Selective ion-exchange intercalation of isomeric dicarboxylate anions into the layered double hydroxide $[LiAl_2(OH)_6]Cl{\cdot}H_2O$, Chem. Mater. 10 (1998) 351–355.
[13] A.M. Fogg, V.M. Green, H.G. Harvey, D. O'Hare, New separation science using shape-selective ion exchange intercalation chemistry, Adv. Mater. 11 (1999) 1466–1469.
[14] F. Cavani, F. Trifiro, A. Vaccari, Hydrotalcite-type anionic clays: preparation, properties and applications, Catal. Today 11 (1991) 173–301.
[15] G.R. Williams, D. O'Hare, Towards understanding control and application of layered double hydroxide chemistry, J. Mater. Chem. 16 (2006) 3065–3074.
[16] W.Y. Shi, M. Wei, L. Jin, C.J. Li, Calcined layered double hydroxides as a "biomolecular vessel" for bromelain: immobilization, storage and release, J. Mol. Catal. B: Enzym. 47 (2007) 58–65.
[17] A.I. Khan, L. Lei, A.J. Norquist, D. O'Hare, Intercalation and controlled release of pharmaceutically active compounds from a layered double hydroxide, Chem. Commun. (2001) 2342–2343.
[18] M.D. Arco, E. Cebadera, S. Gutierrez, C. Marten, M.J. Montero, V. Rives, J. Rocha, M.A. Sevilla, Mg, Al layered double hydroxides with intercalated indomethacin: synthesis, characterization and pharmacological study, J. Pharm. Sci. 93 (2004) 1649–1658.
[19] S. Vial, V. Prevot, F. Leroux, C. Forano, Immobilization of urease in ZnAl layered double hydroxides by soft chemistry routes, Micropor. Mesopor. Mater. 107 (2008) 190–201.
[20] V. Ambrogi, G. Fardella, G. Grandolini, M. Nocchetti, L. Perioli, Effect of hydrotalcite-like compounds on the aqueous solubility of some poorly water-soluble drugs, J. Pharm. Sci. 92 (2003) 1407–1418.
[21] F. Peter, Old and new substrates in clinical nutrition, J. Nutr. 128 (1998) 789–796.
[22] M. Luthra, D. Ranganathan, S. Ranganathan, D. Balasubramanian, Racemization of tyrosine in the insoluble protein fraction of brunescent aging human lenses, J. Biol. Chem. 269 (1994) 22678–22682.
[23] (a) M. Wei, M. Pu, J. Guo, J.B. Han, F. Li, J. He, D.G. Evans, X. Duan, Intercalation of L-dopa into layered double hydroxides: enhancement of both chemical and stereochemical stabilities of a drug through host–guest interactions, Chem. Mater. 20 (2008) 5169–5180;
(b) M. Wei, Q. Yuan, D.G. Evans, Z.Q. Wang, X. Duan, Layered solids as a "molecular container" for pharmaceutical agents: L-tyrosine-intercalated layered double hydroxides, J. Mater. Chem. 15 (2005) 1197–1203.
[24] K.K. Peh, C.F. Wong, Polymeric films as vehicles for buccal delivery: swelling, mechanical and bioadhesive properties, J. Pharm. Pharm. Sci. 2 (1999) 53–61.
[25] P.M. Nguyen, N.S. Zacharia, E. Verploegen, P.T. Hammond, Extended release antibacterial layer-by-layer films incorporating linear-dendritic block copolymer micelles, Chem. Mater. 19 (2007) 5524–5530.
[26] B.-S. Kim, S.W. Park, P.T. Hammond, Hydrogen-bonding layer-by-layer-assembled biodegradable polymeric micelles as drug delivery vehicles from surfaces, ACS NANO 2 (2008) 386–392.
[27] R.P. Bontchev, S. Liu, J.L. Krumhansl, J. Voigt, T.M. Nenoff, Synthesis, characterization, and ion exchange properties of hydrotalcite $Mg_6Al_2(OH)_{16}(A)_x(A')_{2-x}{\cdot}4H_2O$ (A, A′ = Cl^-, Br^-, I^-, and NO_3^-, $2 \geq x \geq 0$) derivatives, Chem. Mater. 15 (2003) 3669–3675.
[28] A.S. Bookin, V.I. Cherkashin, V.A. Drits, Polytype diversity of the hydrotalcite-like minerals. II. Determination of the polytypes of experimentally studied varieties, Clays Clay Miner. 41 (1993) 558–564.
[29] A.P. Mariko, F. Claude, J.P. Besse, Delamination of layered double hydroxides by use of surfactants, Chem. Commun. 1 (2000) 91–92.
[30] Y. Li, H. Li, M. Wei, J. Lu, L. Jin, pH-Responsive composite based on prednisone-block copolymer micelle intercalated inorganic layered matrix: structure and in vitro drug release, Chem. Eng. J. 151 (2009) 359–366.
[31] L. Li, S.P. Schwendeman, Mapping neutral microclimate pH in PLGA microspheres, J. Control. Release 101 (2005) 163–173.
[32] C. Wischke1, S.P. Schwendeman, Principles of encapsulating hydrophobic drugs in PLA/PLGA microparticles, Int. J. Pharm. 364 (2008) 298–327.
[33] C.R. Young, C. Dietzsch, M. Cerea, T. Farrell, K.A. Fegely, A. Rajabi-Siahboomi, J.W. McGinity, Physicochemical characterization and mechanisms of release of theophylline from melt-extruded dosage forms based on a methacrylic acid copolymer, Int. J. Pharm. 301 (2005) 112–120.
[34] T. Kodama, Y. Harada, M. Ueda, K. Shimizu, K. Shuto, S. Komarneni, Selective exchange and fixation of strontium ions with ultrafine Na-4-mica, Langmuir 17 (2001) 4881–4886.
[35] U. Costantino, M. Casciola, L. Massinelli, M. Nocchetti, R. Vivani, Intercalation and grafting of hydrogen phosphates and phosphonates into synthetic hydrotalcites and a.c.-conductivity of the compounds thereby obtained, Solid State Ionics 97 (1997) 203–212.